Environ. Sci. Technol. **1999**, *33,* 142−149

Air Emissions from Exposed Contaminated Sediments and Dredged Material

K. T. VALSARAJ,* R. RAVIKRISHNA, B. CHOY,† D. D. REIBLE, L. J. THIBODEAUX, C. B. PRICE,‡ S. YOST,§ J. M. BRANNON,‡ AND T. E. MYERS‡

Department of Chemical Engineering and Hazardous Substance Research Center (South and Southwest), Louisiana State University, Baton Rouge, Louisiana 70803

The sediment-to-air fluxes of two polycyclic aromatic hydrocarbons (phenanthrene and pyrene) and a heterocyclic aromatic hydrocarbon (dibenzofuran) from a laboratory-contaminated sediment and those of three polycyclic aromatic hydrocarbons (naphthalene, phenanthrene, and pyrene) from three field sediments were investigated in experimental microcosms. The flux was dependent on the sediment moisture content, air-filled porosity, and the relative humidity of the air flowing over the sediment surface. The mathematical model predictions of flux from the laboratory-spiked sediment agreed with observed values. The fluxes of compounds with higher hydrophobicity were more air-side resistance controlled. Conspicuous differences were observed between the fluxes from the laboratory-spiked and two of the three field sediments. Two field sediments showed dramatic increases in mass-transfer resistances with increasing exposure time and had significant fractions of oil and grease. The proposed mathematical model was inadequate for predicting the flux from the latter field sediments. Sediment reworking enhanced the fluxes from the field sediments due to exposure of fresh solids to the air. Variations in flux from the lab-spiked sediment as a result of change in air relative humidity were due to differences in retardation of chemicals on a dry or wet surface sediment. High moisture in the air over the dry sediment increased the competition for sorption sites between water and contaminant and increased the contaminant flux.

Introduction

Approximately one-eighth to one-quarter of the National Superfund Priority List sites include contaminated subaquatic sediments (*1*). Approximately 14−28 million cubic yards of contaminated sediments are managed annually (*2*). Confined disposal facilities (CDFs) are used by the U.S. Army Corps of Engineers to dispose contaminated dredged material from shipping channels and harbors in Great Lakes, along the Atlantic and Gulf coasts, and to some extent along the Pacific coast. CDFs are mostly above ground, and are primarily designed to contain the sediment during storage. However, increasing attention is being directed toward the natural pathways for chemicals to leave the CDF and enter the air and water environments (*3*). For most volatile and semi-volatile contaminants, the primary pathway is volatilization into the atmosphere.

In a CDF there are several locales that can be sources of emissions to the atmosphere. Exposed sediment and dredged materials are the major contaminant transfer locales. Basic conceptual models for emission from these locales have been proposed, but no field experimental data exist at the present time to verify these mathematical models (*4*). Increasingly it is being recognized that before a CDF is sited for a contaminated dredged material, proper estimates should be made of the contaminant exposure to humans and biota through both air and water routes. For example, volatile emissions of organic contaminants and other odorous compounds (e.g., hydrogen sulfide, ammonia, mercaptans) that potentially reduce air quality from the Indiana Harbor upland CDF are of concern due to its proximity to a high school and potential adverse health impacts on the safety of site personnel (*5*). Previous laboratory investigations with New Bedford Harbor sediment showed that organic volatiles were emitted when the material was disturbed and exposed to air (*6*). Mathematical models are essential tools in the estimation of risk from CDFs. Before use as a predictive tool, it is imperative that these models are experimentally verified under controlled laboratory and field conditions.

After a sediment is placed in an upland CDF, water loss by evaporation occurs. Atmospheric precipitation (rain, dew, fog) and tidal variations can increase sediment moisture. A sediment undergoing water drainage and subsequent exposure to air leading to evaporation can show significant differences in air emissions over time (*7*). Sediments stored in a CDF will go through cycles of dry and wet conditions. They are also subject to variations in air relative humidity and temperature. The sorptive capacity of a sediment is a strong function of moisture content (*8*). Dry sediments adsorb high concentrations of organic compounds. As the sediment moisture content or air relative humidity increases, the water molecules effectively displace hydrophobic compounds from the sediment and hence decrease the sediment sorptive capacity. Early investigations on soils showed increased partial pressures of pesticides over wet soils compared to dry soils (*9*). Other work on soils include data on vapor-phase transport of organics from soils of different types (*10*−*17*). We reported results of laboratory experiments on the release of semivolatile organic compounds (SOCs) from a wet (saturated) *thin* sediment layer (0.5 cm) over which air of varying relative humidity was passed to simulate conditions that might exist in the surface sediment of a typical CDF during cyclic wet and dry periods (*18*).

In this paper the effects of sediment moisture content, contaminant aging, and the presence of oil and grease on air emissions from contaminated sediments in laboratory microcosms are reported. These data provide the information for site specific evaluations of air emissions following confined disposal of dredged material. Such evaluations can be used to determine the relative merits of different disposal options, mass releases under disposal conditions, and potential air concentrations.

* Corresponding author telephone: (504)388-6522; fax: (504)388-1476; e-mail: valsaraj@che.lsu.edu.

† Department of Chemical Engineering, University of Sydney, NSW, Australia.

‡ Environmental Laboratory, U.S. Army Corps of Engineers, Vicksburg, MS 39180.

§ DynTel Corporation, Vicksburg, MS 39180.

10.1021/es980510h CCC: $18.00
Published on Web 11/24/1998

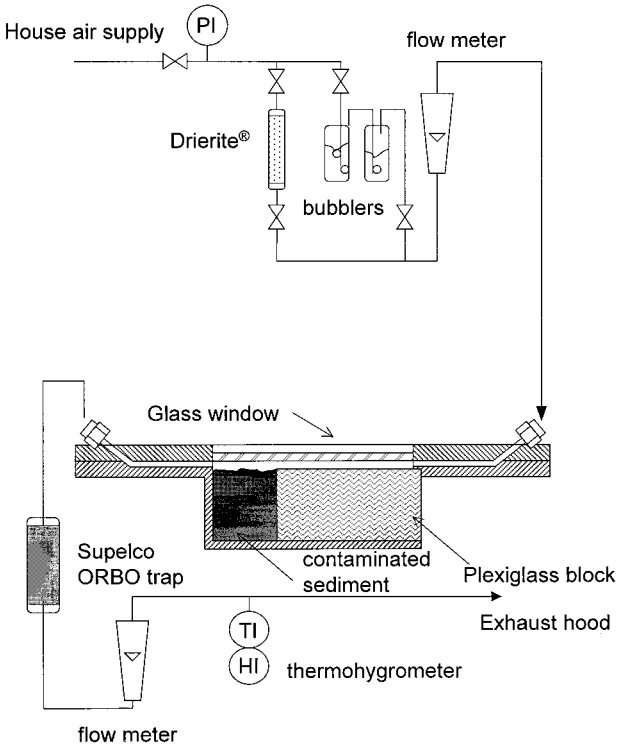

FIGURE 1. Schematic of the microcosm and associated experimental set up.

Experimental Section

Description of Apparatus. A flux chamber constructed of anodized aluminum was used to measure the contaminant fluxes from the sediments (Figure 1). The description of the apparatus is given elsewhere (*18*). Air is supplied to the chamber from a compressed air source at a desired flow rate (1.7 L/min). At the outlet of the chamber, an adsorbent bed (Orbo 43 trap, Supelco, Inc., PA) was used to trap the contaminants from the air stream. A thermohygrometer was used to measure the relative humidity in the outlet air stream.

Contaminants and Sediments. A local uncontaminated sediment (ULS) from the University Lake in Baton Rouge was used as one of the test sediments. It was spiked in the laboratory with the contaminants of interest. Three contaminated sediments from field sites were chosen since these were of interest to the U.S. Army Corps of Engineers. The field sediments were obtained from areas that are planned for sediment dredging and disposal in CDFs. These sediments were (a) IHC sediment obtained from the Indiana Harbor Canal, (b) NYH sediment obtained from the New York Harbor, and (c) GCR sediment obtained from Grand Calumet River, Indiana. The properties of the sediments are given in Table 1.

The contaminants of concern in this work were polycyclic aromatic hydrocarbons (PAHs) and heterocyclic aromatic compounds (HACs) which are two prevalent classes of pollutants in many contaminated sediments. They are semivolatile and hydrophobic and tend to accumulate in the biota. Two PAHs, pyrene (PYR) and phenanthrene (PHE), and one HAC, dibenzofuran (DBF), were the only ones studied in the laboratory-contaminated sediment. Although the field-contaminated sediments contained several compounds (PAHs, polychlorinated biphenyls, hydrogen sulfide, ammonia, mercaptans), only the results on three PAHs (naphthalene, phenanthrene, and pyrene) are reported in this work. The properties of the compounds relevant to this study are given in Table 1.

Preparation of Laboratory-Spiked Sediment. The University Lake (Baton Rouge, LA) sediment was obtained using a box-corer and processed as described earlier (*19*). The sediment was contaminated in the laboratory with phenanthrene, dibenzofuran, and pyrene to the desired loading using a tumbling procedure (*19*). Sodium azide was added to reduce biodegradation of the contaminants. The sediment was prepared by air-drying in a fume hood, crushing, and passing it through a 2 mm sieve to obtain a moisture content of 6.5% (wet basis). The 26% moisture sediment was air-dried first but not crushed or sieved, before adjusting the moisture content. The initial sediment moisture content was determined and the calculated amount of additional water needed was added. The sediment was tumbled for 48 h to ensure uniform moisture.

Preparation of Field Sediments. The IHC and NYH sediments were collected using a vibracore sampler, while the GCR sediment was obtained using a manual piston tube sampler. The GCR and IHC field contaminated sediments were transported in 5-gallon buckets in iced coolers to the Waterways Experiment Station, Vicksburg, MS, and immediately blended in barrels. The sediments were divided again into 5-gallon buckets and stored at 4 °C. NYH sediment was transported in 55-gallon drums which were brought to the WES in a refrigerated truck. They were immediately

TABLE 1. Properties of Sediments and Contaminants[a]

Laboratory-Spiked University Lake Sediment (ULS)		
moisture content, θ_w (% g/g)	6.5	26
fraction organic carbon, f_{oc}	0.03	0.03
bulk density, ρ_b (g/cm^3)	0.74	1.2
sand (%)	3	3
silt (%)	41	41
clay (%)	56	56
total porosity, ϵ_T (cm^3/cm^3)	0.72	0.52
air-filled porosity, ϵ_a (cm^3/cm^3)	0.67	0.03
dibenzofuran (mg/kg)	46	108
phenanthrene (mg/kg)	67	97
pyrene (mg/kg)	55	94

Field-Sediments	**IHC**	**NYH**	**GCR**
moisture content, θ_w (% g/g)	54	53	62
fraction organic carbon, f_{oc}	0.026	0.027	0.054
fraction oil and grease, f_{og}	0.01	0.0003	0.014
bulk density, ρ_b (g/cm^3)	0.6	0.66	0.51
sand (%)	45	57	75
silt (%)	46	37	17.5
clay (%)	8	5	7.5
total porosity, ϵ_T (cm^3/cm^3)	0.78	0.7	0.83
air-filled porosity, ϵ_a (cm^3/cm^3)	0.021	0.07	0.025
cation exchange capacity (meq/g)		0.047	
pH		7.54	6.9
naphthalene (mg/kg)	38	0.2	586
phenanthrene (mg/kg)	51	0.9	432
pyrene (mg/kg)	59	1.9	172
TRPH (mg/kg)	12 790	287	54 000

Contaminant Properties (18,21)	**NAPH**	**DBF**	**PHE**	**PYR**
aqueous solubility (mg/L)	32	10	1	0.15
vapor pressure (mmHg)	0.017	0.0036	0.00025	4.5×10^{-6}
log K_{oc} (L/kg)	3.1	4.0	4.4	4.8
Henry's constant, H_c	0.019	0.0031	0.0025	0.00045
diffusivity in air, D_A, (cm^2/s)	0.062	0.060	0.058	0.054
sediment/air partition constant, K_d*, L/kg				
ULS, wet, log $K_{d,w}$*	3.29	4.87	5.91	6.63
ULS, dry, log $K_{d,d}$*	NA	6.8	8.0	10.0

[a] Abbreviations: NA, not applicable; TRPH, total recoverable petroleum hydrocarbons. $K_{d,w}$* obtained by experimental measurements (*23*). $K_{d,d}$* estimated as in ref *18*. $\epsilon_w = \epsilon_T - \epsilon_a$.

blended in a lysimeter, divided into 5-gallon buckets and stored at 4 °C. Before loading the microcosm the buckets were once again thoroughly mixed. No biocide was added to the field sediment nor was the sediment moisture content adjusted as was done for the lab-spiked ULS. A sub sample was taken for chemical analysis.

Experimental Run. The experimental set up is shown in Figure 1. The width of the sediment cavity in the direction of the air flow can be varied by using different thicknesses of plexiglass as shown in Figure 1. Two such thicknesses (5 and 15 cm) were used in these experiments. A flow rate of 1.7 L/min was chosen upon the basis of earlier investigations (*18*). The contaminant traps were replaced after each sample interval. At the end of the run (ULS) the sediment was sectioned into thin layers and analyzed.

Analytical Methods. The Orbo 43 trap was analyzed for the contaminants of interest. After extraction with acetonitrile the sample was analyzed by high-pressure liquid chromatography (HP 1090) using EPA method 8270 for PAHs (*20*). Moisture content of the sediment sample was measured on a wet basis. Total organic content was reported on a dry basis.

Calculation of Experimental Flux. The experimental flux $N_A(t)$ (ng/cm^2·h) was calculated from the mass of a contaminant collected (Δm_A, ng) in the trap during the duration of time (Δt, h)

$$N_A(t) = \frac{\Delta m_A}{\Delta t A_c} \tag{1}$$

where A_c is the area (cm^2) of the sediment-air interface in the microcosm.

Theory

A Resistance-in-Series Vignette Model. Although the overall process of release and transport of contaminants into air involves complex chemodynamics, for purposes of simplifying and interpreting mechanisms it is convenient to adopt a simple, approximate model (*7*). The process can be visualized to occur via a series of three steps: (a) It commences with the contaminant on the solids of initial uniform loading, W_A (mg/kg) existing in equilibrium with pore air, giving initial concentration $C_A{}^o = W_A/K_d{}^*$, where $K_d{}^*$ is the sediment−air partition constant for the contaminant (L/kg), (b) diffusion of the contaminant through the air-filled pore spaces to the sediment−air interface, and (c) finally convective transport through the air-side boundary layer before it emerges into bulk air. Thus there is particle-to-air phase partitioning followed by two transport resistances before a contaminant enters the atmosphere. The flux from the sediment to the atmosphere is given by (*7*)

$$N_A = \frac{(C_A{}^o - C_A{}^*)}{\frac{1}{k_a} + \sqrt{\frac{\pi t}{D_e R_f}}} \tag{2}$$

where $C_A{}^*$ is the background concentration in the atmosphere (ng/cm^3), and k_a is the mass transfer coefficient on the air side of the interface (cm/s). D_e is the effective diffusivity (cm^2/s) given by the Millington-Quirk expression (*7*), $D_A\epsilon_a{}^{10/3}/\epsilon_T{}^2$. ϵ_a is the air-filled porosity of the sediment and ϵ_T is the total sediment porosity. R_f is the retardation factor for the contaminant on the sediment and is given by $\epsilon_a + (\epsilon_w/H_c) + \rho_b K_d{}^*$. $K_d{}^*$ is the sediment−air partition constant for the contaminant (L/kg). The value of $K_d{}^*$ varies with the moisture content. For a "wet" sediment (>4% moisture content by weight), unless direct experimental measurements are available, it can be estimated from $K_d{}^* = K_{oc}f_{oc}/H_c$. H_c is the air−water partition constant (Henry's law constant, dimensionless molar ratio), K_{oc} is the organic carbon-based sediment−water partition constant for the chemical (L/kg), and f_{oc} is the fraction organic carbon in the sediment. ρ_b is the sediment bulk density (g/cm^3). The sediment moisture content affects both D_e and R_f. For a "dry" sediment (<1% sediment moisture content), $\epsilon_w \approx 0$. A "dry" sediment will have a large R_f since $K_d{}^*$ for a "dry" sediment is considerably larger than that for the "wet" sediment. A "dry" sediment will also have a large D_e as given by $D_A\epsilon_a{}^{4/3}$.

Because of widely varying chemical species concentrations in bed-sediments the process is clarified if measured fluxes are normalized to source concentrations. In doing so, eq 2 can be rewritten, for clean background air ($C_A{}^* = 0$)

$$\frac{C_A{}^o}{N_A} = \frac{1}{k_a} + \sqrt{\frac{\pi t}{D_e R_f}} \tag{3}$$

In the above rearrangement, the ratio $C_A{}^o/N_A$ is seen to be the measure of the overall mass transfer resistance capturing the entire process of chemical release and movement in the multimedia system. The right hand side of eq 3 represent two resistances in series. In its conventional interpretation $1/k_a$ is termed the air-side resistance and $[(\pi t)/(D_e R_f)]^{1/2}$ is the sediment-side resistance although it contains both thermodynamic and transport parameters.

As inspection of eq 3 shows that during early times, $t \rightarrow 0$, the chemical flux is dominated by R_{air}, the air-side resistance. However, as time increases R_{sed}, the sediment-side resistance increases in magnitude until the sediment side resistance controls. The resistance-in-series model has, however, some important predictions about chemical release and transport that are counterintuitive. The first one is that as the hydrophobicity increases the rate of chemical emission to air is increasingly controlled by R_{air}, the air-side resistance. Equation 3 clearly shows that as R_f increases, $C_A{}^o/N_A \approx 1/k_a$. The other transport implication of the vignette model is that for large times, $t \rightarrow \infty$, irrespective of R_f, the sediment-side resistance controls the emission rate.

Using the resistance-in-series concept a purely sediment-side transport process employing semi-infinite slab transport diffusion equation is coupled with the film model for the air side, effectively eliminating the unknown but variable interface concentration, $C_{Ai}(t)$. Some small error results using this approach; the next section contains the exact model and compares the two.

The Exact Chemodynamic Model. For the sediment microcosm geometry described in the Experimental Section and the associated boundary conditions for the diffusion process, the following exact analytical equation for the pore-air concentration, $C_A(z,t)$, and flux to air, $N_A(t)$ (*21*, *22*), can be obtained

$$C_A(z,t) = C_A{}^o\left[\operatorname{erf}\left(\frac{R_f z}{\sqrt{4D_e R_f t}}\right) + \exp\left(\frac{k_a z}{D_e} + \frac{k_a{}^2 t}{D_e R_f}\right)\operatorname{erfc}\left(\frac{R_f z}{\sqrt{4D_e R_f}} + k_a\sqrt{\frac{t}{D_e R_f}}\right)\right] \tag{4}$$

$$N_A(t) = C_A{}^o k_a \exp\left(\frac{t}{\tau}\right)\operatorname{erfc}\left(\sqrt{\frac{t}{\tau}}\right) \tag{5}$$

The time constant τ is given by $(D_e R_f)/k_a{}^2$. z (cm) is the distance downward from the sediment surface. For $t \rightarrow 0$, $N_A = k_a C_A{}^o$ and for $t \rightarrow \infty$

$$N_A(t) = C_A{}^o\sqrt{\frac{D_e R_f}{\pi t}}$$

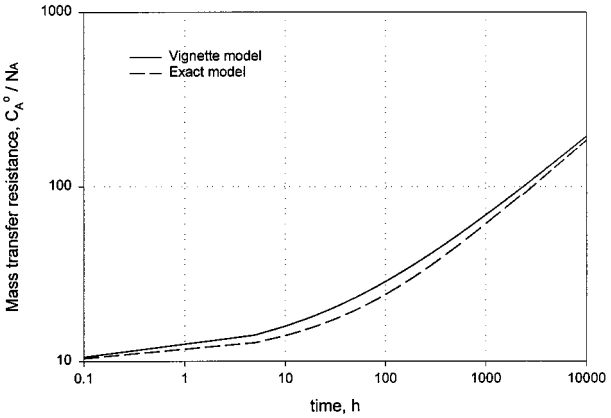

FIGURE 2. Comparison of mass transfer resistances predicted by the vignette and exact chemodynamic models. Parameters used for illustration are for DBF in 6.5% moisture ULS from Table 1.

Similarly, as $k_a \rightarrow \infty$ (no air-side resistance) the flux is purely diffusion controlled and is given by

$$N_A(t) = C_A^o \sqrt{\frac{D_e R_f}{\pi t}} \qquad (6)$$

A description of the models and MATHCAD templates are available on the Internet at the following address: (http://www.chem.eng.usyd.edu.au/pgrad/bruce/). The above equations including 5 and 6 are consistent with the approximate vignette model presented previously. However in eq 5 the resistances R_{air} and R_{sed} are impossible to distinguish. Numerical computations comparing the mass transfer resistance C_A^o/N_A for both models appear in Figure 2 using the parameters for DBF in 6.5% moisture ULS for illustration (Table 1). The models predict identical values for both initial time ($t = 0$) and for long times ($t \rightarrow \infty$). The maximum deviation is observed at intermediate time periods and is <15%.

Experimental Results and Discussion

Effects of Sediment Moisture, Contaminant Hydrophobicity, and Air-Side Resistance. Figure 3, parts a−c represents the flux of DBF, PHE, and PYR from the laboratory spiked ULS. The first experiment with 6.5% moisture content was run with humidified inlet air (99% relative humidity). For a sediment with moisture content at or above 6.5% we observed in separate experiments that the pore air was saturated with water vapor (*23*). Hence in this case there was no loss of moisture from the sediment. In the second experiment with 26% moisture content, since the wet sediment was in contact with incoming dry air−water loss from the sediment was appreciable. However, for the duration of the contaminant flux measurement (336 h) in the second experiment, the water flux was constant (~0.45 mg/cm²·h). Moisture content of the surface sediment did not vary significantly, and it remained relatively "wet" during the course of the test. This observation was significant since it assured us that the retardation of the chemicals in the sediment remained unchanged during the course of these experiments. In both cases sediment compaction was insignificant.

The flux of DBF from the sediment is shown in Figure 3a. For the 6.5% moisture sediment, the flux decreased from a high value of 120 ng/cm²·h to a steady-state value of 50 ng/cm²·h after 300 h. However, for the 26% moisture sediment, the initial flux was 110 ng/cm²·h at 6 h and decreased rapidly to 18 ng/cm²·h in 336 h. Clearly, the long-term flux from the 26% moisture sediment was lower than from the 6.5% moisture sediment. For the latter case, the predicted fluxes for DBF under two separate conditions are shown, one where the surface mass transfer coefficient was assumed to be infinite ($k_a \rightarrow \infty$, eq 6) and the second for a finite mass transfer coefficient ($k_a = 0.08$ cm/s, eq 5) as predicted by the boundary layer theory (*18*). In the case of DBF, it was obvious that assuming $k_a \rightarrow \infty$ gave a better fit to the data, indicating that its mass transfer was not air-side resistance controlled. Decreasing k_a to 0.08 cm/s increased the air-side mass transfer resistance slightly and predicted a smaller flux than observed. The effect of k_a on the flux was evident only during the early stages of the experiment, beyond this time period the emission is controlled increasingly by the sediment side. The same conclusions also applied to the 26% moisture sediment. The primary difference between the simulations for the two sediments was due to changes in air-filled porosity which in turn changed the effective diffusivity in the models. The calculated value of D_e for DBF in the 6.5% moisture ULS (0.020 cm²/s) was 454 times larger than the D_e for 26% moisture ULS (4.4×10^{-5} cm²/s). This was due to the very low air-filled porosity in the latter case (see data in Table 1).

Figure 3b shows the flux of PYR from both sediments. For the 6.5% moisture sediment, the initial flux was 2.95 ng/cm²·h and thereafter remained constant at ~2.8 ng/cm²·h. The model assuming $k_a \rightarrow \infty$ vastly over predicted the experimental flux, whereas that for a k_a of 0.076 cm/s (obtained from boundary layer theory) was in excellent agreement with the experimental data. This is consonant with the earlier comment regarding the overall resistance, R_{Total}. Compounds with large K_d* (or large R_f) will have small $R_{sed}(t)$ and R_{air} will become significant. The air-phase resistance is, therefore, quite significant in controlling the flux of PYR. The conclusion is the same for the 26% moisture sediment. Even though $R_{air} > R_{sed}$ the latter contributes somewhat so that as with DBF, pores occupied with water causes a lower flux, 0.2 vs 0.1 ng/cm²·h at 600 h.

For PHE, Figure 3c shows that the flux is large in the beginning (51 ng/cm²·h) for the 6.5% moisture sediment and gradually decreased to 20 ng/cm²·h in 293 h. For the 26% moisture case, the initial flux was 11.4 ng/cm²·h which sharply decreased to 0.9 ng/cm²·h in 122 h. In both cases the model assuming an infinite k_a, showed better agreement with the data. Like DBF, due to its relatively low R_f, the flux of PHE is sediment side controlled except when time is zero.

Figure 3d shows the sediment concentration profile after 35 days of the experiment with 6.5% moisture ULS. Significant depletion of DBF and PHE was noted in the top 30- and 10-mm layers respectively of the surface sediment. The deeper layers had concentrations identical to the initial loadings. The final sediment concentration profiles predicted from $W_A(z) = C_A(z)K_d$* with $C_A(z)$ using eq 4 are also given in Figure 3d. There is good agreement between the model and observed values. That the predictions of both fluxes (Figures 3a,c) and final sediment concentration profiles (Figure 3d) are a priori and contain no adjustable parameters, indicate the robustness of the model and the appropriateness of the assumptions inherent in it. The sum of the mass of compound collected in the overflowing air and the mass remaining in the sediment was compared to the initial sediment loading. Mass balances of 93% for DBF and 96% for PHE were accounted for in this manner.

Differences between Lab-Spiked and Field Sediments. Apart from the aging time difference of the laboratory and field samples, two of the latter (IHC and GCR) contained substantial fractions of oil and grease (f_{og} of 0.01 and 0.014, respectively). The NYH field sediment had insignificant oil and grease (f_{og} of 0.0003) and the laboratory-spiked ULS had none. The presence of oil and grease, apparently had a dramatic effect on the fluxes from the sediments. Figure 4, parts a b, compare the overall mass transfer resistance for NAPH and PYR from the four sediments studied. Although

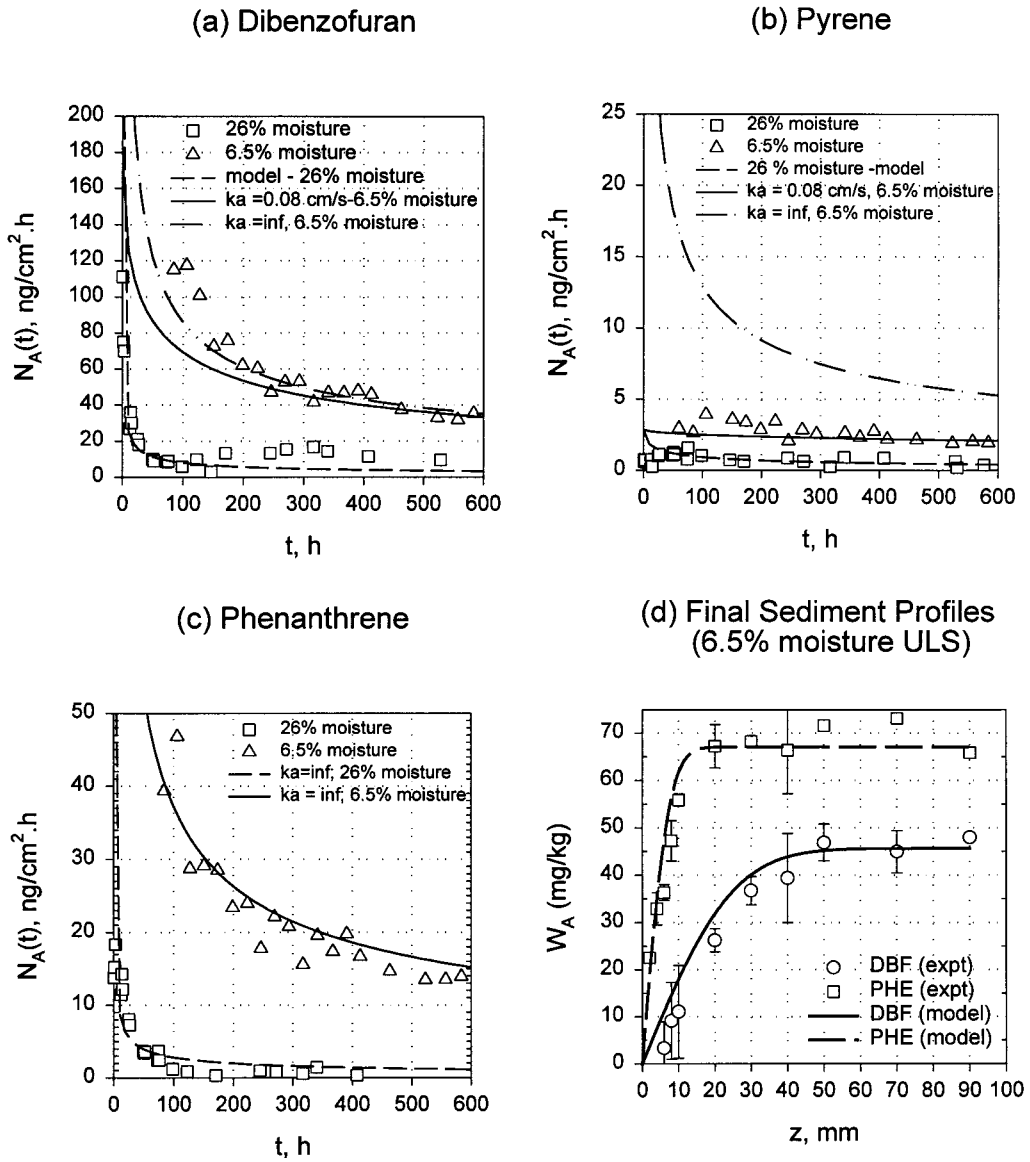

FIGURE 3. Flux of (a) dibenzofuran (DBF), (b) pyrene (PYR), and (c) phenanthrene (PHE) from the 6.5% and 26% moisture ULS. The theoretical curves are from eqs 3 and 4 with the following D_e (values in cm^2/s):

	DBF	PHE	PYR
6.5% moisture	**0.020**	**0.029**	**0.027**
26% moisture	**4.4×10^{-5}**	**4.4×10^{-5}**	**4×10^{-5}**

The weighted sum of squared residuals $\sum_i((N_t^{exp} - N_t^{model})/N^{model})^2$ was 0.3, 0.35, and 0.76 respectively for DBF, PHE, and PYR for the 6.5% moisture case. (d) Experimental and model predicted concentration profiles of DBF and PHE in the 6.5% moisture content ULS after 35 days of experimental run.

experiments were conducted for all three PAHs (NAPH, PHE, and PYR), to reduce clutter only the data for NAPH and PYR are shown here. Whereas NAPH had the highest flux, PYR had the smallest, and PHE was intermediate between the two. Figure 4a is the comparison of mass transfer resistance for ULS and NYH sediments, both of which had little or no oil and grease associated with them, while Figure 4b is for the two remaining sediments (GCR and IHC) which contained significant fractions of oil and grease. The comparisons were for identical experimental design. In all cases dry air at a flow rate of 1.7 L/min was passed over the sediment surface. The experiments were conducted at high sediment moisture contents (53−62%) for the field sediments, and compared to the lab-spiked sediment (ULS) at a high moisture content (26%).

To interpret the data we chose the chemodynamic vignette model in the form of eq 3. Theoretical computations of this three-step model are possible using the properties in Table 1. The results of the computations appear as solid lines in Figure 4a using the D_e and K_d* data for naphthalene on NYH and pyrene on both NYH and ULS. The resistance-in-series model predicts evaporative behavior strongly related to hydrophobicity. All pore-air diffusivities are similar in magnitude, but R_f (PYR) > R_f (NAPH). Due to the large R_f for PYR, eq 3 dictates that its resistance will be the lowest and dominates for 30 h by conductance through the air layer above the sediment. Beyond 30 h the sediment-side resistance for PYR commences to influence the flux. Naphthalene is less hydrophobic, and its flux is controlled by the resistance on the sediment side over the entire time period of 1 to 1000 h. Figure 4a shows that the predicted values of resistance for PYR on ULS also followed this behavior.

Figure 4b shows that for NAPH and PYR the measured mass transfer resistance in the two field sediments (IHC and

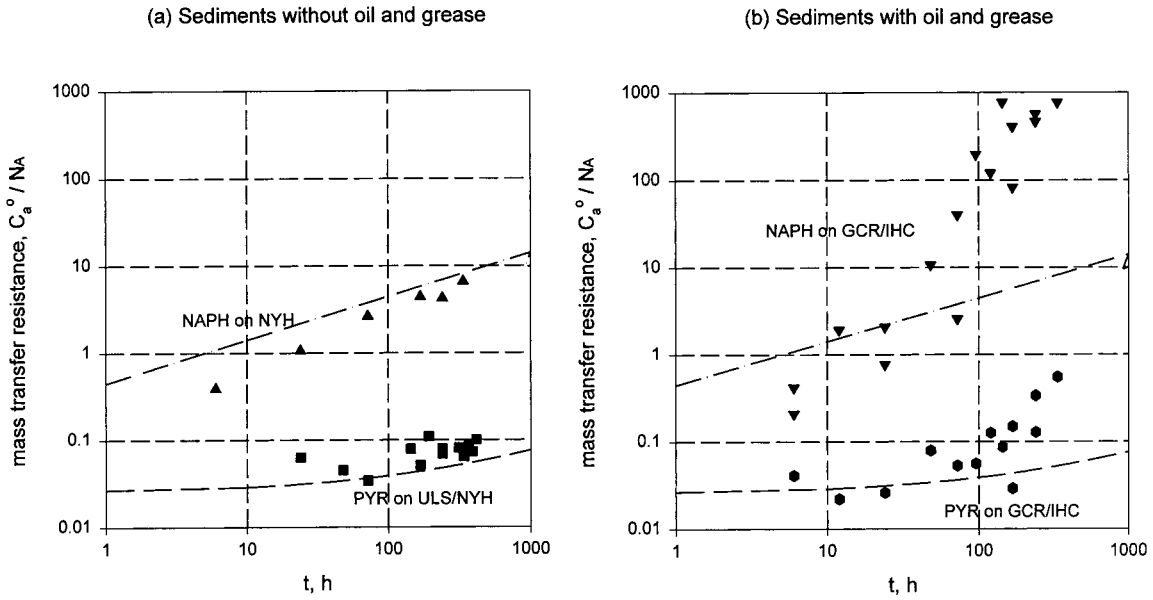

FIGURE 4. Model predicted and experimental resistances for the mass transfer of pyrene and naphthalene from (a) sediments without oil and grease (laboratory-spiked ULS and field contaminated NYH) and (b) oil and grease containing sediments (IHC and GCR).

GCR) showed deviations from the resistance-in-series model beyond about 30 h of evaporation time. Up until that time the behavior followed the theory displaying small R_{sed} values (slope of 0.5); however, beyond this time the resistances for both compounds increased dramatically. The same occurred with PHE, but it is not shown here. The magnitude of the overall resistance for NAPH was larger than either PHE or PYR for both sediments. It is evident that the behavior of the oil and grease containing sediments vis-à-vis those that do not contain any appreciable amounts of oil and grease are clearly different. The dramatic increase in resistance at long times is indicative of additional mass transfer resistances.

We hypothesize that the oil and grease present in GCR and IHC gave rise to the additional mass transfer resistance. The physical model was based on a previous experiment on the effects of oil and grease on sediment-to-water transport of PAHs (*24*). It was observed in the experiment that the oil and grease accumulated at the bed sediment−water interface at approximately twice the concentration than at the bottom of the flux chamber cell. The same argument can be advanced in the present experiments. Toward the beginning of the test, soon after the wet, contaminated sediment is placed in the microcosm, the oil and grease fraction will migrate to the surface due to buoyancy differences. With the loss of water from the saturated sediment through evaporation into the air flowing over it, this will lead to a high oil and grease concentration in the upper surface sediment layer. The contaminant present in the oil and grease evaporates quickly upon exposure to air; further transport has to occur by diffusion through the depleted oil layer which provides an additional mass transfer resistance. Since diffusion through the oil will be much slower owing to its higher viscosity ($D_A \propto \mu^{-1}$) (*22*), the flux will diminish rapidly to negligible values. It is expected that a similar process would occur on placement of oil and grease containing sediments in a CDF.

Effect of Sediment Reworking. The experiment with field-contaminated sediments was designed to provide information on maximum contaminant fluxes expected under site management conditions which might occur in a CDF. To simulate this, the sediment was subject to reworking within the chamber. After passing dry air over the wet sediment (cycle 1), the sediment was rewetted to field capacity and reworked in a glovebag (*5*). Thereupon dry air was again passed over the wet sediment (cycle 2). It was observed that during cycle 2, the flux of PAHs increased to levels similar to that during cycle 1 and decayed similarly. For example, Figure 5a,b shows the comparison of fluxes for NAPH from GCR and IHC respectively during the two cycles. The fluxes were of similar magnitude in both cycles. We also observed that for the contaminated bed sediments from field sites, as long as they remained "wet", neither variations in air relative humidity nor rewetting to original field capacity resulted in significant changes in flux. Only the physical disturbance of the sediment through reworking brought about large increases in fluxes as shown in Figure 5a,b. Sediment reworking brings fresh sediment, oil and grease to the surface and hence leads to increase in flux. In a CDF, during the filling stage which lasts from several months to years reworking is an inevitable operation. Hence one should expect significant air pollution during initial sediment exposure (after placement) and after periodic reworking activities which expose underlying material.

Effect of Air Relative Humidity. Figure 6a−c shows the effect of changing air relative humidity on the flux of DBF, PHE, and PYR from the laboratory-spiked ULS. Initially the sediment was "wet" (6.5% moisture content) with a saturated water vapor concentration in the sediment pore air. Humid (water saturated) air was passed over the sediment. Since the air was water saturated, there was no water flux out of the sediment. Both inlet and outlet air showed 99+% relative humidity. The flux in this case (run 1) showed a classic diffusive profile with a relatively large initial value. After 650 h of run 1, the humid air was replaced with dry air over the sediment (run 2). Since the air was now unsaturated compared to the sediment pore space, the water flux increased and quickly declined to a very small value after 840 h of the run (Figure 6d). The fluxes of DBF, PHE, and PYR decreased, reaching steady state in a short time. After 840 h of the experiment, the dry air was changed back to humid air (run 3). The water flux was negligible, while the flux of all compounds increased. The flux reestablished upon changing to humid air (run 3) was an extrapolation of that from run 1. Clearly, the flux was large when air relative humidity was high. During run 2, water loss from the surface created a drying surface sediment which had a higher sorption capacity for the chemicals as observed in earlier experiments from our laboratory on a thin (0.5 cm) sediment layer (*18*). These observations are similar to those reported for vola-

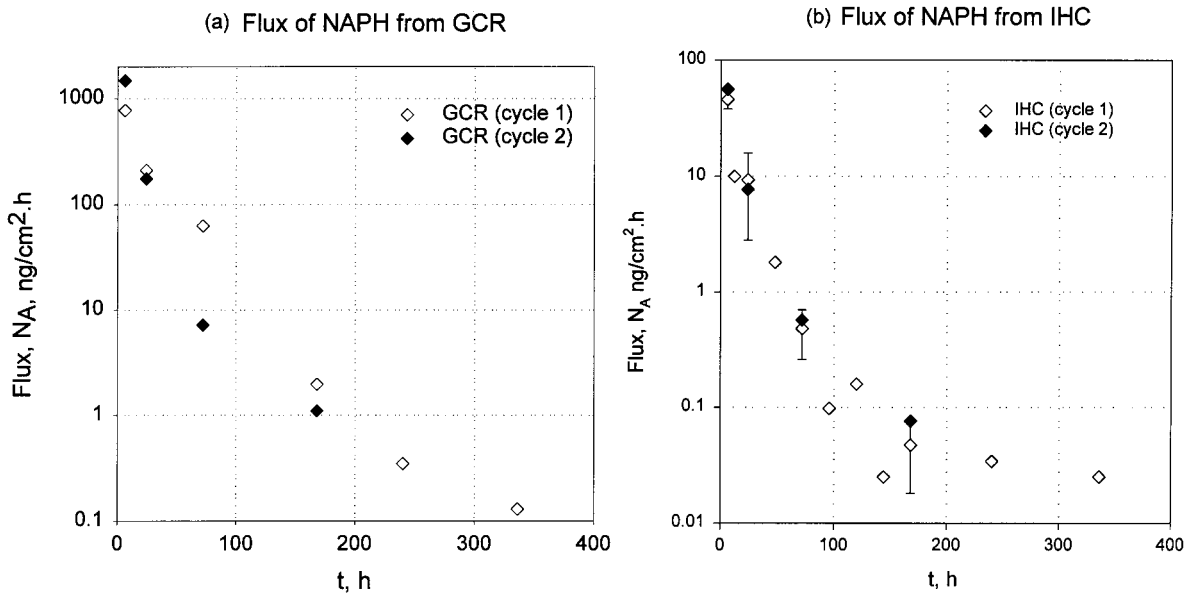

FIGURE 5. Effect of sediment reworking on naphthalene flux from (a) GCR and (b) IHC sediments during the two cycles.

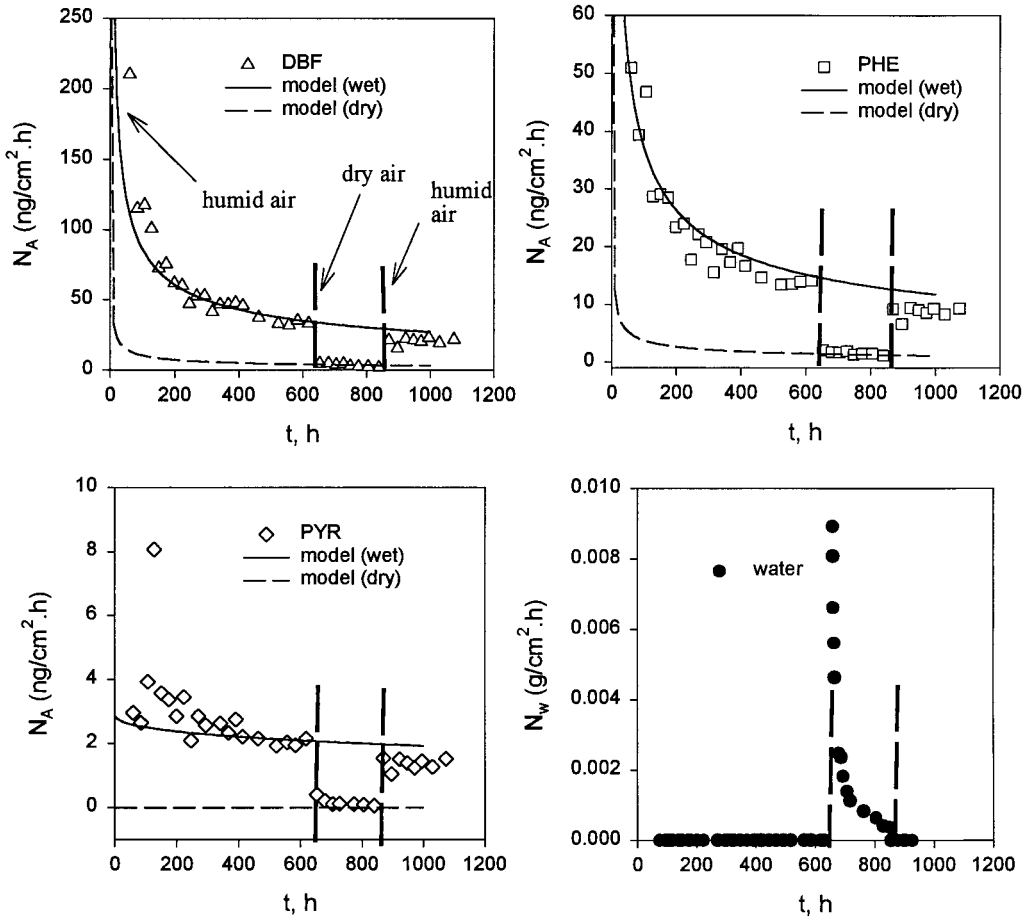

FIGURE 6. Effect of change in air relative humidity on dibenzofuran, phenanthrene, pyrene, and water flux from 6.5% moisture ULS. Model curves for humid air over "wet" sediment conditions are the same as in Figure 2. For the case of dry air over "dry" sediment the following D_e (cm²/s) values were used: DBF (0.036), PHE (0.037), and PYR (0.038). Other parameters used are in Table 1.

tilization of pesticides from agricultural soils (*8, 17*). As PAHs diffused out of the sediment, they were adsorbed to the dry surface sediment layer. Upon termination of run 2, therefore, the pore-air concentration in the surface layers would be low. The beginning of run 3 will increase the pore-air concentration since the air relative humidity is high and water will displace some sorbed PAHs. This increases the flux so that the pore-air concentration will quickly reestablish that during the latter stages of run 1. Cyclic changes in air relative humidity and sediment moisture are very likely in a CDF as it undergoes diurnal patterns of wet and dry periods. On the basis of our observations we should anticipate that the air concentrations near a CDF will be large during a humid atmospheric condition following a dry period.

Figure 6a−c also shows the model predictions. In the first simulation it was assumed that the sediment moisture remained at or above those of the "wet" sediment throughout the run and hence the retardation factors remained constant during the run. Also shown is another simulation assuming that the sediment was "dry" even from the beginning. The "wet" sediment model is the same as that described previously and used in Figure 3a−c. For the "dry" sediment, the values of D_e and R_f are different. The model for flux from the "dry" sediment is also given by eq 5. The values of K_d* used in the "dry" sediment model for the compounds are given in Table 1. These simulations show the relative fluxes to be expected from a "dry" or a "wet" sediment. The steady-state flux upon changing to dry air was in line with the predictions for the dry sediment model, indicating that our assumptions of surface drying and enhanced sorption are substantially correct.

Acknowledgments

This work was funded by the U.S. EPA through the Hazardous Substances Research Center (South and Southwest) and by the U.S. Army Corps of Engineers.

Literature Cited

(1) Wall, T. Overview of Management Strategies for Contaminated Sediments; *Workshop on Contaminated Sediments and the Gulf of Mexico*, August, 27−29, **1991**, New Orleans, LA.

(2) National Research Council. *Contaminated Sediments in Ports and Waterways- Cleanup Strategies and Technologies*, National Academy Press: Washington, DC, 1997.

(3) US EPA, *Estimating Contaminant Losses from Components of Remediation Alternatives for Contaminated Sediments*, EPA 905-R96−001, Great Lakes National Program Office, Chicago, IL, March, 1996.

(4) Valsaraj, K. T,; Thibodeaux, L. J.; Reible, D. D. In, *Dredging, Remediation and Containment of Contaminated Sediments*, ASTM STP 1293, K. R. Demars; G. N. Richardson; R. N. Yong; and R. C. Chaney, Eds., ASTM, Philadelphia, **1995;** pp 227−238.

(5) Price, C. B. *Laboratory Assessment of Volatilization from Indiana Harbor Sediment*, Memorandum for Record CEWES-ES−P, U S Army Corps of Engineer Waterways Experiment Station, Vicksburg, MS, September 1997.

(6) Brannon, J M. *Laboratory Assessment of Volatilization from New Bedford Harbor Sediment*, Memorandum for Record, WESES-A, US Army Engineer Waterways Experiment Station, Vicksburg, MS, April 1989.

(7) Thibodeaux, L. J. *Theoretical Models for Volatile Emissions from Dredged Material − Comparison of Predicted and Laboratory Measurements for New Bedford Harbor Sediment*, Memorandum for Record, WESES-A, U. S. Army Engineer Waterways Experiment Station, Vicksburg, MS, August 1989.

(8) Valsaraj, K. T.; Thibodeaux, L. J. *J. Haz. Mater.* **1988**, *19*, 79−100.

(9) Spencer, W. F.; Farmer, W. J.; Jury, W. A. *Environ. Toxicol. Chem.* **1982**, *1*, 17−26.

(10) Ryan, P. A.; Cohen, Y. *Soil Sci. Soc. Am. J.* **1990**, *54*, 341−346.

(11) Chiou, C. T.; Shoup, T. D. *Environ. Sci. Technol.* **1985**, *19*, 1196−1200.

(12) Erkey, C. T.; Campagnolo, J. F.; Akgerman, A. *Sep. Purif. Methods* **1995**, *24*, 129-.

(13) Lindhardt, B.; Christensen, T. H.; Andersen, L. *Water, Air Soil Poll.* **1996**, *89*, 129−146.

(14) Lindhardt, B.; Christensen, T. H. *Water, Air and Soil Poll.* **1996**, *92*, 375−389.

(15) Jury, W. A., Russo, D., Streile, G., and El Abd, H. *Water Res. Res.* **1990**, *26*: 13−20.

(16) U. S. E P A: *EMSOFT- Exposure Model for Soil − Organic Fate and Transport User's Guide*, EPA/600/C-97/001, U. S. EPA-ORD, Washington, D. C., February, 1997.

(17) Taylor, A. W., Spencer, W. F. Chapter 7 in *Pesticides in the Soil Environment − Processes, Impacts and Modeling*, H. Cheng (Editor), Soil Science Society of America, Madison, WI, 1990, pp 213−269.

(18) Valsaraj, K. T.; Choy, B.; Ravikrishna, R.; Reible, D. D.; Thibodeaux, L. J.; Price, C. B.; Brannon, J. M.; Myers, T. E. *J. Haz. Mater.*, **1997**, *54*, 65−87.

(19) Thoma, G. J., Ph.D. Dissertation, Louisiana State University, Baton Rouge, LA, 1994.

(20) U S EPA, *Test Methods for Evaluating Solid Waste Physical/Chemical Methods*, Third Edition, Final Update III Method 8310, U. S. GPO, Washington, D.C. December, 1996.

(21) Ravikrishna, R.; Valsaraj, K. T.; S. Yost.; Price, C. B.; Brannon, J. M. *J. Haz. Mater.*, **1998**, *60*, 89−104.

(22) Choy, B.; Reible, D. D. *Contaminant Transport in Soils and Sediments*: *Mathematical Analysis*, Report to the EPA Hazardous Substance Research Center (S&SW), Louisiana State University, Baton Rouge, LA, November, 1997.

(23) de Seze G, Valsaraj K T, Reible D D and Thibodeaux L J., Paper 518 presented at the symposium on Interfaces in Environmental Chemistry and Toxicology, Eighth Annual Meeting of SETAC−Europe, Bordeaux, France, April 14−18, 1998.

(24) Luong, T T., M.S. Thesis, Louisiana State University, Baton Rouge, LA, 1996.

Received for review May 19, 1998. Revised manuscript received October 6, 1998. Accepted October 16, 1998.

ES980510H